Polymer Testing 111 (2022) 107590

Contents lists available at ScienceDirect

Polymer Testing

journal homepage: www.elsevier.com/locate/polytest

Matricial foaming

Daniele Tammaro [a], Valerio Loianno [a], Fabrizio Errichiello [b,c], Ernesto Di Maio [a,c,*]

[a] Dipartimento di Ingegneria Chimica, dei Materiali e della Produzione Industriale, University of Naples Federico II, P.le Tecchio 80, I-80125, Naples, NA, Italy
[b] Materias S.r.l., Corso Nicolangelo Protopisani, 50, I-80146, Naples, NA, Italy
[c] foamlab, University of Naples Federico II, P.le Vincenzo Tecchio, 80, I-80125, Naples, NA, Italy

ARTICLE INFO

Keywords:
Gas foaming
Experiment matrix
Foaming temperature
Pressure drop rate
Multi-group experiments
High throughput experimentation

ABSTRACT

We designed an innovative pressure vessel for a high throughput study of batch foaming of thermoplastic polymers. With the new pressure vessel, the foaming process can be conducted concurrently on sixteen samples (arranged in a 4 × 4 wells matrix) at four different temperatures and at four different pressure drop rates, at the same saturation pressure. We herein describe the design principle, the working conditions and the first results gathered on poly(ε-caprolactone) samples foamed with carbon dioxide as the blowing agent. We explored the processing variables space: foaming temperature in the range 30–40 °C; pressure drop rate in the range 1–5 MPa/s; saturation pressure fixed at 5 MPa within a single experiment. The expected dependence of density as well as morphology on processing variables proves the suitability of the method for the high throughput study of novel polymers and can be utilized for the fast development of resins suitable for foaming.

1. Introduction

Recently, the use of polymeric foams is increasingly growing in different application fields as their structural and functional properties are being implemented by the introduction to the market of new polymers having improved properties, reduced costs, or augmented sustainability [1,2]. Among the processing methods to produce foams, gas foaming is the most popular, and technologies adopting gas foaming, namely extrusion, injection molding and steam chest molding, are highly productive [3–8]. Gas foaming consists in allowing the evolution of a gaseous phase within a compliant polymer (e.g.: in the rubbery or molten state) after inducing a supersaturation state in a polymer/gas solution [9,10].

To control the density and the morphology of the foamed samples, the processing variables are to be fine-tuned to exploit the specific features of the neat polymer and the characteristics of the polymer/blowing agent, BA, solution [11,12]. The correlation among processing variables [13], polymer properties [14], foam structure [15] (in terms of density and pore morphology) and final properties has been the focus of a huge number of papers and efforts in the scientific community for the complexity, the heterogeneity, and the economic importance of the outcomes [16–18].

Between the 1980s and 2000s, the gas foaming key processing variables were rationalized as being: i) the foaming temperature, T_{foam}; ii) the gas amount within the solution, e.g.: in terms of the weight fraction, x_{gas} [19]; iii) the rate at which the polymer/BA solution is brought to the supersaturation state, e.g.: by pressure quenching a high-temperature polymer/BA solution - hence the pressure drop rate, PDR [20]. T_{foam} is the most important processing variable to define the final foam structure both in terms of density and morphology [2]. For instance, a bell-shaped curve typically describes the effect of T_{foam} on the foam density, with a density minimum at optimal foaming temperature. Above the optimal T_{foam}, the reduction of the polymer viscosity induces the occurrence of bubbles coalescing mechanisms responsible for the loss of the BA and reduction of foaming efficiency. Below the optimal T_{foam}, either the viscosity rise or the crystallization or vitrification take place earlier, and hinder bubble growth. The two other foaming processing variables, PDR and x_{gas}, are usually both maximized: a larger PDR induces finer morphologies and higher foaming efficiency, while a larger x_{gas} induces lower densities and finer morphologies [21]. Of course, both are upper bounded by the processing equipment (e.g.: maximum design pressure and gas evacuation rate capability), while x_{gas} is also limited by the maximum expansion that the polymer can withstand before coalescence [22].

To reduce the number of experiments to map the relationship between processing variables and foam features (in terms of foam density

* Corresponding author. Dipartimento di Ingegneria Chimica, dei Materiali e della Produzione Industriale, University of Naples Federico II, P.le Tecchio 80, I-80125, Napoli, Italy.
E-mail address: edimaio@unina.it (E. Di Maio).

https://doi.org/10.1016/j.polymertesting.2022.107590
Received 2 January 2022; Received in revised form 27 March 2022; Accepted 16 April 2022
Available online 30 April 2022

and morphology), different approaches were adopted, encompassing the enlightenment of the key processing variables as well as the design of new experimental procedures or tools [23,24]. Design-of-Experiment statistical methods, linearization of the effects (keeping the experimental window narrow) [25] as well as the decoupling of effects were some of the adopted approaches [18]. From a purely experimental point of view, the group of prof. Kiran [19] introduced a pressure vessel capable of achieving a temperature gradient to a long-strip shaped sample, to conduct foaming tests at the same pressure and PDR and at different temperatures in a single experiment.

In this context, we herein introduce a further development of the latter, a purely experimental approach to explore multiple foaming conditions in a single foaming experiment. In particular, we designed a foaming equipment consisting of a pressure vessel having several reaction chambers disposed as rows and columns in a matrix style, from which the term "matricial foaming". Each chamber allows setting a different T_{foam} and/or PDR at uniform saturation conditions fixed by the constant partial pressure of the BA. By considering that different x_{gas} are achieved when conducting the gas solubilization at the same saturation pressure but at different temperatures, in this way, we explore the whole processing variable dimensionality. The matricial foaming experiment requires only a few polymer granules and is of critical importance when designing new polymers in a high throughput approach [26,27].

2. Materials and methods

Poly(ε-caprolactone), PCL (CAPA 6800, Perstorp, Cardiff by the Sea, CA, USA), a biodegradable polyester of fossil origin, was adopted as a model polymer for testing the validity of the approach. Basic properties of interest to the foaming process are presented in Table 1. As received, the granules have an average diameter of ca. 3 mm. Technical grade CO_2 was supplied by SOL S.p.A. (Monza, Italy).

The foams were characterized to determine their bulk density (ρ) and cell density (N). ρ was measured according to ASTM D7710, using an analytical balance (Mettler Toledo, Columbus, OH). The cellular structure of the foams was investigated by using a scanning electron microscope (Hitachi TM 3000 SEM). N was calculated as $N=(\rho_p/\rho)\, n^{3/2}$, where n is the number of cells in the area A of the SEM micrograph and ρ_p is the density of the solid sample. The cell size was measured according to ASTM D3576.

2.1. Foaming apparatus

The pressure vessel is a three-piece, cylindrical stainless steel, custom-designed autoclave, produced by Roman Weber GmbH (Tobel, Switzerland), schematized in Fig. 1. The bottom piece (in Fig. 1-bottom and in Fig. 2b) includes 16 cylindrical sample wells, 15 mm in diameter and 15 mm in height, 4 of which (on a diagonal) are equipped with a pressure and temperature (T_{melt}) transducer (KE2-6-M-B35D, Gefran S.p.A., Provaglio d'Iseo, Brescia, Italy). Fig. 2 reports some images of the parts and the assembly. On the two sides of the 16 wells, 2 through holes per side are present for housing the heating cartridges. One cartridge per side includes a type-J thermocouple for temperature control ($T_{control}$ – blue-wired in Fig. 2). The cartridges allow to reach a maximum temperature of 540 °C, however, in the present stage, Viton O-ring define the working temperature range between ambient temperature and a maximum temperature of 200 °C. The control, here and correspondingly on the top piece, is such to induce a linear temperature gradient in the wells, in one direction, forming 4 isotherm wells-lines, each at different temperatures. Heat dissipation is hindered by using layers of insulating material (polytetrafluoroethylene) between the base of the apparatus and the wooden base box beneath and between the lid of the apparatus and the piston of the press Moreover, for testing at high temperatures, additional thermal insulation layers can be assembled to assure a suitable heat loss control. The details of the linear temperature gradient are discussed in greater detail in SI.

Table 1
Properties of Poly(ε-caprolactone) (commercial name CAPA 6800).

M_W (mass average molar mass)	T_g (°C)	T_m (°C)	ρ (g/cm^3) @ 0.1 MPa, 25 °C
80000	−60	60	1.140

The central piece is a disk with 4 lines of holes corresponding vertically to the 16 wells. Each line contains 4 holes of 1, 2, 4 and 8 mm in diameter (hole size variation – see yellow arrow in Fig. 2c). These are the holes for the escape of the BA from each well. The different hole diameter is responsible for BA escape from the well at different velocities and causing, consequently, different PDR in the wells. The central piece is assembled on the bottom piece in such a way that the hole gradient is perpendicular to the temperature gradient (Fig. 2c). In this way, each polymer sample in the 16 wells experiences a different T_{foam} or a different *PDR*. The use of 4 pressure and temperature sensors located diagonally beneath the four wells (Fig. 1d) allows for estimating the foaming conditions in the remaining 12 wells. The top piece contains the connections to the BA dosing (¼"NPT) and the BA evacuation (½"NPT) along with the two sets of cartridge housing, similarly to the bottom piece. Dosing is performed via a KB 15 high-pressure coaxial valve (Müller co-ax AG, onwards called *input valve*). Evacuation is performed via an actuated ball valve (15–71 NFB and 15–72 NFB TSR8, High Pressure Equipment Co., Erie, PA, USA, onwards called *output valve*). Both valves are normally closed. To keep the samples at the desired temperature imposed by the heating cartridges, copper wells of 14 mm diameter and 10 mm height are used to host the samples within the base wells. The overall reaction cell has a diameter of 14 mm and a height of 3.6 mm. Both the bottom and central part of the assembly have a circumferential outer cavity on their top surface each of which hosts an O-ring made of Viton. Fig. 1d shows the sensor positions within the top and bottom pieces: heat cartridges are marked in green, temperature sensors are marked in red and pressure sensors are marked in blue.

The top piece is connected to the piston head of a 10-ton press (VLP Bench Frame, Enerpac, New Brunswick, NJ, USA), which guarantees BA pressure tight closure of the autoclave. The press and the assembly are reported in Fig. 3. Fig. 2d shows the closed autoclave with the piston in full stroke position. The three parts of the cell are aligned so that no additional operation is needed to close it, but the force applied by the pump. In this configuration the maximum working pressure of the blowing agents is defined by the clamping force of the hydraulic press used to secure the closing of the apparatus. The 10-ton press limit and the area of the apparatus set the maximum pressure to 5.0 MPa.

A multifunction-controller 3850T from Gefran S.p.A. (Provaglio d'Iseo, Brescia, Italy) was used to control heating ($T_{control}$ and heating cartridges) and measuring plus recording T_{melt} and pressures during the whole test. From these data the PDR at pressure release is easily evaluated. The controller was also utilized to actuate the dosing and evacuation valves. The apparatus is enclosed in a polycarbonate cage during the experiments to secure the operation. Fig. 1c and d show 2D views of the bottom piece, in which the samples are placed.

The design of pressure drop in different holes can be achieved by tuning the size of the restriction that hinders the gas evacuation. As instance, an analytical solution for the depressurization of a high-pressure tank was developed by Guo et al. [28].

2.2. Foaming protocol

At room temperature and pressure, the autoclave is opened, and each well is filled with a granule of PCL as received from the supplier. After positioning the central disk on the bottom part, the assembly is closed with the hydraulic pump by applying a force of 10 tons. The output valve is closed, and vacuum purging is applied from the input valve to dry the sample and remove any contaminant for 1 h at room temperature. The two valves are closed and the Gefran 3850T PID control is enabled to

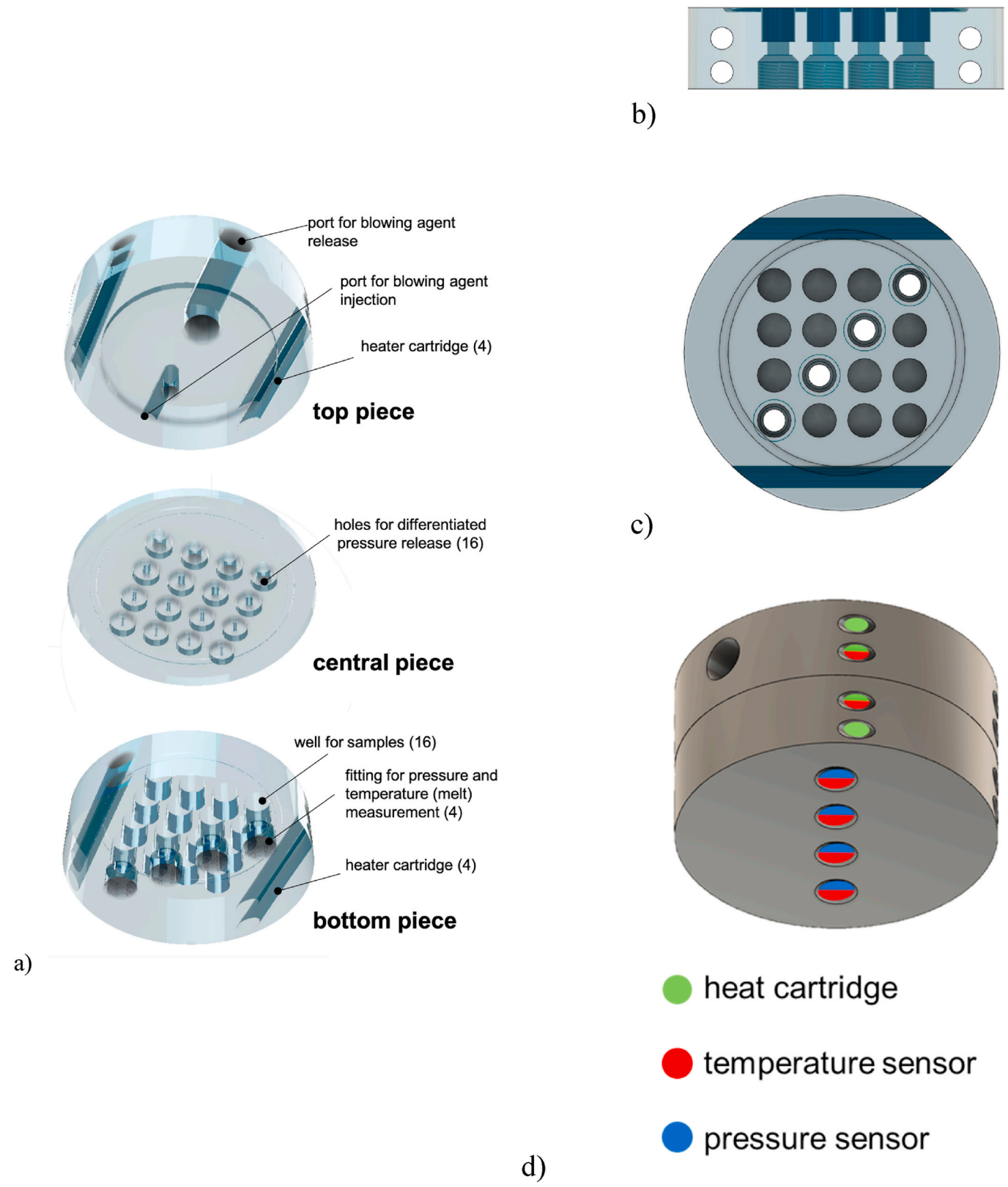

Fig. 1. a) 3D renderings of the top, central and bottom pieces of the matricial equipment; b) 2D lateral view of the bottom piece; c) 2D top view of the bottom piece; d) sketch of the equipment illustrating the position of: heating cartridges (green marks), temperature sensors (red marks) and pressure sensors (blue marks). . (For interpretation of the references to colour in this figure legend, the reader is referred to the Web version of this article.)

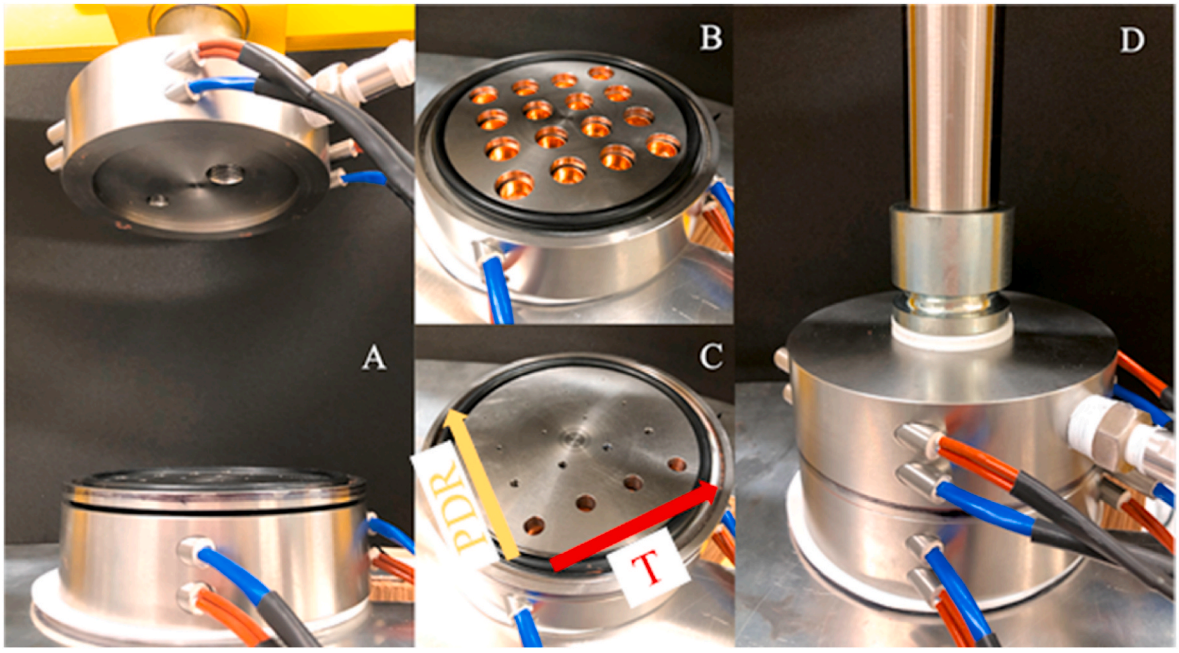

Fig. 2. Pictures of the assembled pressure vessel and details of the pieces: (a), open configuration; (b), details of the bottom piece with the 4 × 4 wells and copper sample holders; (c), central piece assembled on the bottom piece, showing the pressure discharge holes for the different PDRs (PDR gradient orthogonal to the T_{foam} gradient); (d), closed configuration.

Fig. 3. Picture of the overall assembly showing the 10-ton press, the blowing agent connections, ports and valves.

establish the desired temperature gradient within the assembly. Thus, the first foaming experiment totally replicates the literature protocol: the assembly is heated up to 70 °C and, after reaching thermal equilibrium, the cell is filled with carbon dioxide up to 4.0 MPa. The system is kept at the chosen thermodynamic conditions for 2 h to reach thermodynamic equilibrium. T_{melt} and pressure are recorded during the entire process. The system is quenched at T_{foam} equal to 43 °C from one side in ca. 10 min and the pressure is kept constant by opening the input valve. This step enables the solidification of the previously molten polymer and does not affect the carbon dioxide concentration within it. Indeed, sorption of low MW gas in thermoplastic polymers is an exothermic process but the diffusion time is much higher than the quenching time. Last, the output valve is open and PCL pellets foam.

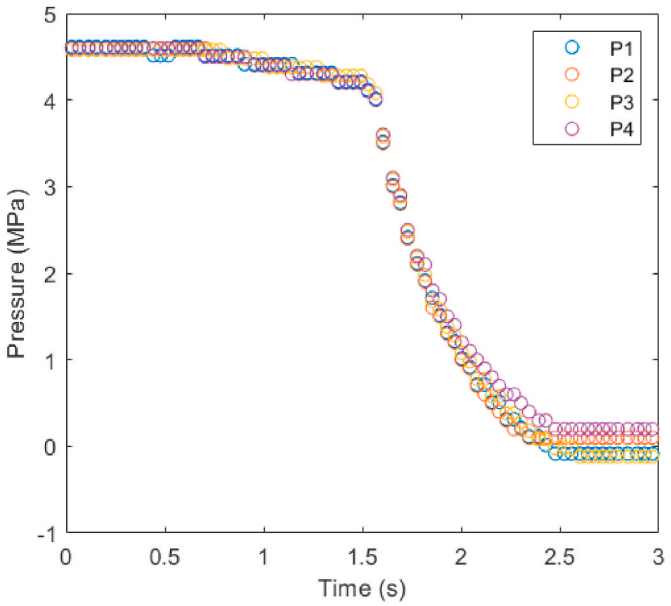

Fig. 4. Pressure drop histories at the different measurement points.

Fig. 4 compares the pressure as a function of time in the diagonal wells: the PDR is evaluated as $PDR = \frac{DP}{Dt}$, where DP is the total pressure drop (i.e., 4.7 MPa) and Dt is the total time of the depressurization (i.e., 0.9, 1.1, 1.4, 1.8 s). Although the PDR measurement is only performed in four wells along the gradient direction, the PDR in the remaining 12 chambers is well approximated by the measured values. Indeed, this parameter only depends on the central disk holes diameter.

3. Results and discussion

The resulting foams, following the foaming protocol, are shown in Fig. 5. The analysis of the 16 samples, obtained with one single test, confirms the strong dependency of the foaming process on the foaming temperature. The effect of different T_{foam} is immediately visible in Fig. 5, where the whiter foams present a lower density and a finer morphology. The effect of the PDR on the rows within the same T_{foam} is less clear by a first visual inspection.

A single test with the matricial batch allows to build a surface plot of the foam density and crystallinity on the whole range of processing conditions investigated, i.e., from 29.5 °C to 39 °C and from 2 to 4.1 MPa/s, (Fig. 6). The 16 PCL foams have density ranging from 78 to 486 kg/m^3, and the surface plot in Fig. 6a reveals that, in the range of temperature and PDR investigated, the dependence of the density on the T_{foam} is stronger than on PDR. A slight decrease of density is observed by increasing the PDR at fixed T_{foam} and it becomes clearer at low foaming temperature of 29.5 °C, where doubling the PDR (from 2 to 4 MPa/s) the foam density passes from 110 to 78 kg/m^3. The density increases monotonically as a function of the T_{foam}, pointing out that the reduction of the polymer viscosity induces the occurrence of bubbles coalescing mechanisms responsible for the loss of the BA and reduction of foaming efficiency.

The crystallization and melting of PCL were measured using a Perkin–Elmer differential scanning calorimeter (DSC 2B), calibrated from the enthalpy of fusion of a known mass of indium. Random sections of the foamed PCL pellets with a weight of ca. 5 mg were contained in aluminum pans, and an empty pan was used as a reference. Melting traces were obtained by heating from 290 to 350 K at 10 K/min. The degree of crystallinity was calculated as follows, a linear baseline was drawn from the first onset of melting to the last trace of crystallinity and the enthalpy of fusion was then calculated from the area under the endotherm. The weight fraction degree of crystallinity (X_c) was defined as:

$$X_c = \frac{\Delta H}{\Delta H_0}$$

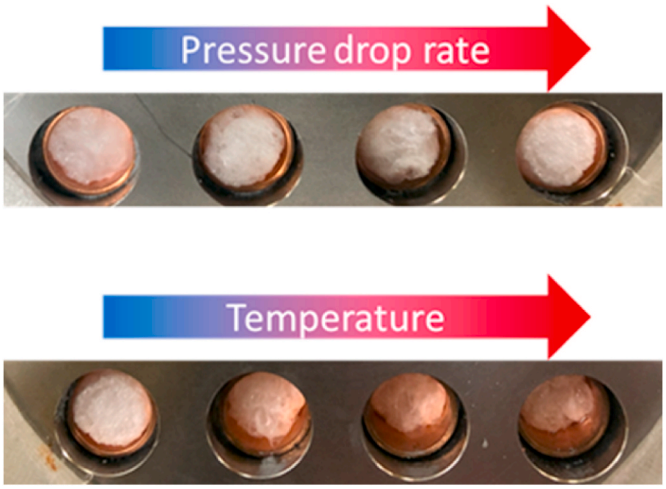

Fig. 5. PCL foams with matricial foaming.

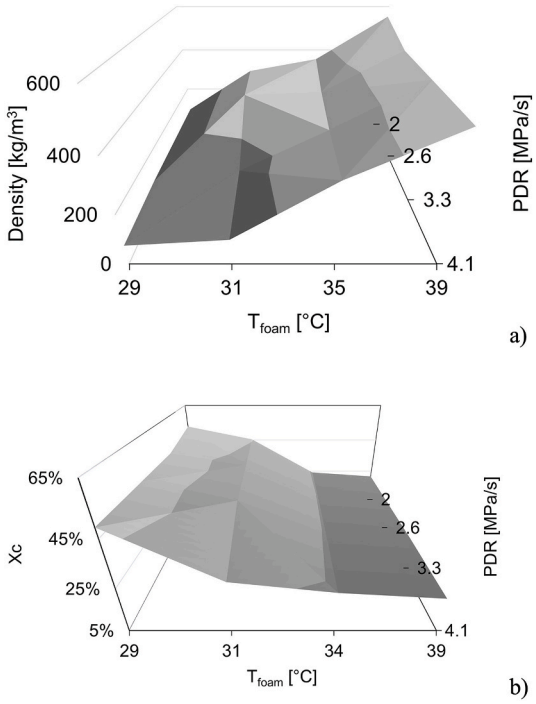

Fig. 6. (a) Foaming map of the density; (b) the weight fraction degree of crystallinity, X_c, as function of processing parameters obtained in one single experiment by matricial foaming.

Where ΔH is the enthalpy of fusion measured at the melting point and ΔH_0 is the enthalpy of fusion of completely crystalline PCL equal to 139.3 J/g (taken from Ref. 26). The measured map of X_c is shown in Fig. 6b where the effect of PDR and T_{foam} can be seen. The X_c varies slightly over the PDR range investigated, the biggest variation is measured at $T_{foam} = 31$ °C where X_c increases from 36% to 39% passing from 4 to 2 MPa/s. The T_{foam} has a strong effect on X_c, at 2 MPa/s the X_c decreases as a function of T_{foam} passing from at 53% at 29 °C to 21% at 39 °C. Incredibly, the entire 3D map of crystallinity can be obtained with one single experiment.

A closer look of the foam morphology by SEM reveals the finer effect of the different PDR (Fig. 7). The results in Fig. 7a show the cell morphology for two rows of samples at different PDR and different temperatures produced in one foaming test. The irregularity of the morphology is due to the presence of welding lines among the pellets inserted in each well. The cellular morphology of the foams in the four diagonal wells (i.e., where T1, T2, T3 and T4 are measured) is shown in Fig. 7b. The cell size is strongly dependent on the foaming temperature, i.e., the sample closer to the hot cartridge has the coarser morphology and vice versa.

The cellular morphologies in Fig. 7 are in good agreement with the morphology obtained by conventional batch foaming [29] in terms of cell size and foam density.

4. Conclusions

We reported the design of a pressure vessel for the high throughput study of batch foaming of thermoplastic polymers. Two important foaming variables, temperature and PDR, were changed simultaneously in each test performing 16 samples that map the foamability of a polymer/BA couple at 4 different temperatures and PDR. The resulting foams of PCL/CO_2 are analyzed in terms of density and cell morphology. The possibility to collect data using a high throughput experimentation (HTE) allows an effective optimization of the foaming process and to speed up innovation all along the knowledge and value chains for

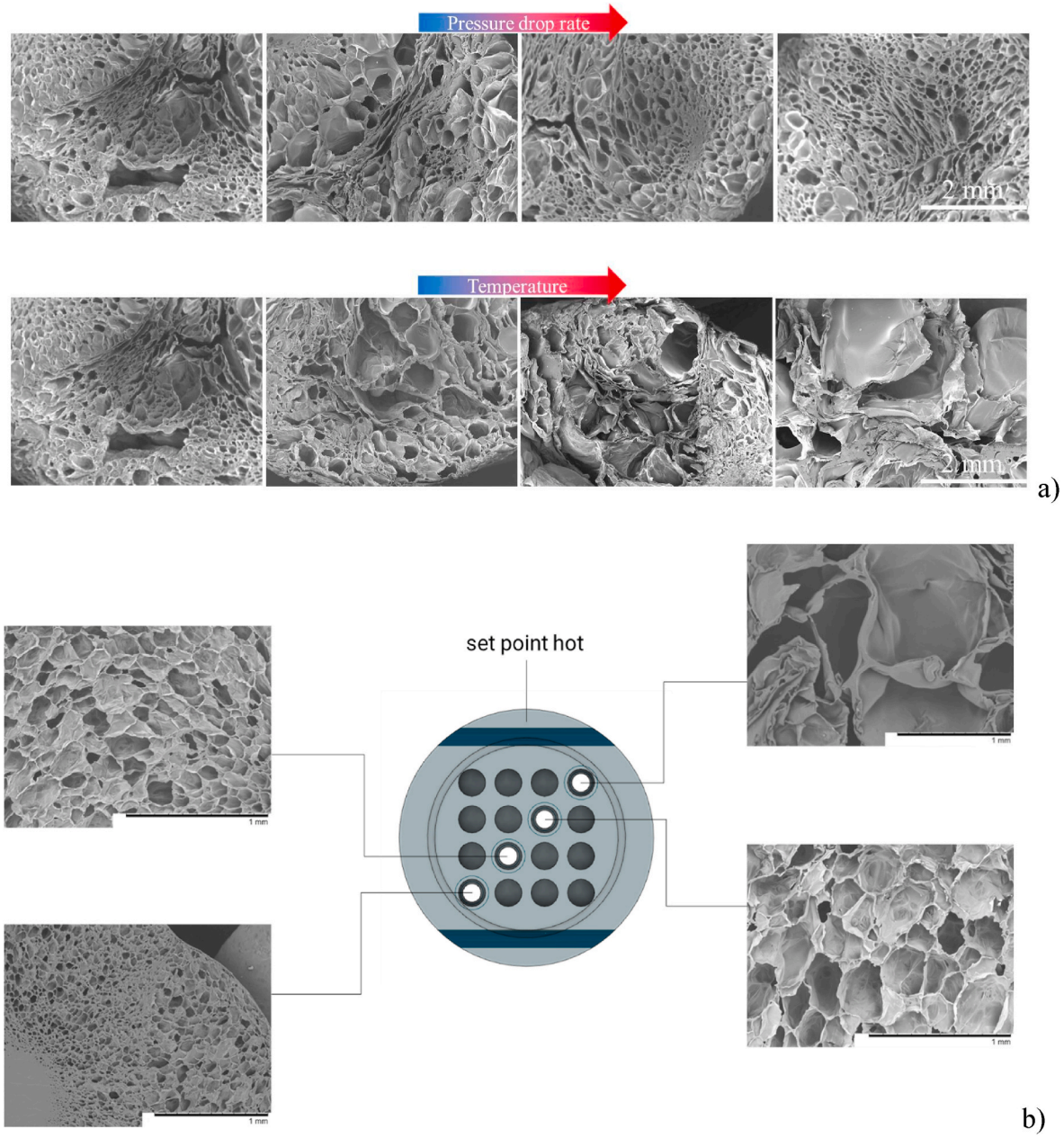

Fig. 7. a) SEM of PCL foams produced by one experiment in the matricial batch; b) cellular morphology of the samples in 4 diagonal wells represented by pictures acquired via SEM (x100 magnification).

polymer foaming. HTE is a technology for running very large numbers of miniaturized experiments (hundreds or thousands per day) in the parallel mode under robotic control. The results can be fed into stochastic computational models that identify structure-properties relationships (SPR) with the aid of Machine Learning tools.

Data availability statement

The data that support the findings of this study are available from the corresponding author, EDM, upon reasonable request.

Authors statement

All authors have participated sufficiently in the conception and design of this work or the analysis and interpretation of the data, as well as the writing of the manuscript, to take public responsibility for it. All authors believe the manuscript represents valid work. All authors have reviewed the final version and approved it for publication. Neither this manuscript nor one with substantially similar content under our authorship has been published or is being considered for publication elsewhere.

Declaration of competing interest

The authors declare that they have no known competing financial interests or personal relationships that could have appeared to influence the work reported in this paper.

Appendix A. Supplementary data

Supplementary data to this article can be found online at https://doi.org/10.1016/j.polymertesting.2022.107590.

References

[1] E. Di Maio, S. Iannace, G. Mensitieri, Ongoing research and future research challenges, in: Foam. With Supercrit. Fluids, Supercrit. Fluid Sci. Techn^{ol}., first ed., Elsevier, 2021, pp. 433–459, https://doi.org/10.1016/B978-0-444-63724-6.00014-7.

[2] T. Standau, C. Zhao, S.M. Castellón, C. Bonten, V. Altstädt, Chemical modification and foam processing of polylactide (PLA), Polymers 11 (2019), https://doi.org/10.3390/polym11020306.

[3] H.O. Pham Hoai Nam, Pralay maiti, masami okamoto, tadao kotaka, takashi nakayama, mitsuko takada, masahiro ohshima, arimitsu usuki, naoki hasegawa, foam processing and cellular structure of polypropylene/clay nanocomposites, Polym. Eng. Sci. 42 (2002) 1907–1918, https://doi.org/10.1002/pen.11083.

[4] E. Di Maio, S. Iannace, G. Mensitieri, Foam technologies, in: Foam. With Supercrit. Fluids, Supercrit. Fluid Sci. Techn^{ol}., first ed., Elsevier, 2021, pp. 21–32, https://doi.org/10.1016/B978-0-444-63724-6.00003-2.

[5] C.D. Han, C.A. Villamizar, Studies on structural foam processing I. The rheology of foam extrusion, Polym. Eng. Sci. 18 (1978) 687–698, https://doi.org/10.1002/PEN.760180904.

[6] C. Fan, C. Wan, F. Gao, C. Huang, Z. Xi, Z. Xu, L. Zhao, T. Liu, Extrusion foaming of poly(ethylene terephthalate) with carbon dioxide based on rheology analysis. https://doi.org/10.1177/0021955X14566085, 2015, 52 277-298.

[7] T. Ishikawa, K. Taki, M. Ohshima, Visual observation and numerical studies of N 2 vs. CO 2 foaming behavior in core-back foam injection molding, Polym. Eng. Sci. 52 (2012) 875–883, https://doi.org/10.1002/pen.22154.

[8] C. Ge, Q. Ren, S. Wang, W. Zheng, W. Zhai, C.B. Park, Steam-chest molding of expanded thermoplastic polyurethane bead foams and their mechanical properties, Chem. Eng. Sci. 174 (2017) 337–346, https://doi.org/10.1016/j.ces.2017.09.011.

[9] I. Tsivintzelis, G. Sanxaridou, E. Pavlidou, C. Panayiotou, Foaming of polymers with supercritical fluids: a thermodynamic investigation, J. Supercrit. Fluids 110 (2016) 240–250, https://doi.org/10.1016/j.supflu.2015.11.025.

[10] D. Miller, V. Kumar, A design-of-experiment study on the microcellular extrusion of sub-critical CO 2 saturated PLA pellets, Int. Polym. Process. 26 (2011) 517–524, https://doi.org/10.3139/217.2467/MACHINEREADABLECITATION/RIS.

[11] D.F. Baldwin, M. Shimbo, N.P. Suh, The role of gas dissolution and induced crystallization during microcellular polymer processing: a study of poly (ethylene terephthalate) and carbon dioxide systems, J. Eng. Mater. Technol. 117 (1995) 62–74, https://doi.org/10.1115/1.2804373.

[12] D.L. Tomasko, A. Burley, L. Feng, S.K. Yeh, K. Miyazono, S. Nirmal-Kumar, I. Kusaka, K. Koelling, Development of CO2 for polymer foam applications, J. Supercrit. Fluids 47 (2009) 493–499, https://doi.org/10.1016/j.supflu.2008.10.018.

[13] C.B. Park, A.H. Behravesh, R.D. Venter, Low density microcellular foam processing in extrusion using CO2, Polym. Eng. Sci. 38 (1998) 1812–1823, https://doi.org/10.1002/PEN.10351.

[14] R. Liao, W. Yu, C. Zhou, Rheological control in foaming polymeric materials: II. Semi-crystalline polymers, Polymer (Guildf). 51 (2010) 6334–6345, https://doi.org/10.1016/j.polymer.2010.11.001.

[15] C.B. Park, D.F. Baldwin, N.P. Suh, Effect of the pressure drop rate on cell nucleation in continuous processing of microcellular polymers, Polym. Eng. Sci. 35 (1995) 432–440, https://doi.org/10.1002/pen.760350509.

[16] F.A. Shutov, Integral/Structural Polymer Foams, 1986. Integr. Polym. Foam, https://link.springer.com/book/10.1007/978-3-662-02486-7.

[17] G. Wu, P. Xie, H. Yang, K. Dang, Y. Xu, M. Sain, L.S. Turng, W. Yang, A review of thermoplastic polymer foams for functional applications, J. Mater. Sci. 5620 (56) (2021) 11579–11604, https://doi.org/10.1007/S10853-021-06034-6, 2021.

[18] C. Marrazzo, E. Di Maio, S. Iannace, Foaming of synthetic and natural biodegradable polymers, J. Cell. Plast. 43 (2007), https://doi.org/10.1177/0021955X06073214.

[19] M.T. Ngo, J.S. Dickmann, J.C. Hassler, E. Kiran, A new experimental system for combinatorial exploration of foaming of polymers in carbon dioxide: the gradient foaming of PMMA, J. Supercrit. Fluids 109 (2016) 1–19, https://doi.org/10.1016/j.supflu.2015.09.030.

[20] D. Tammaro, A. Astarita, E. Di Maio, S. Iannace, Polystyrene foaming at high pressure drop rates, Ind. Eng. Chem. Res. 55 (2016) 5696–5701, https://doi.org/10.1021/acs.iecr.5b04911.

[21] M.R. Barzegari, D. Rodrigue, The effect of injection molding conditions on the morphology of polymer structural foams, Polym. Eng. Sci. 49 (2009) 949–959, https://doi.org/10.1002/PEN.21283.

[22] L.S. Turng, H. Kharbas, Effect of process conditions on the weld-line strength and microstructure of microcellular injection molded parts, Polym. Eng. Sci. 43 (2003) 157–168, https://doi.org/10.1002/PEN.10013.

[23] D. Tammaro, V. Contaldi, M.G.P. Carbone, E. Di Maio, S. Iannace, A novel lab-scale batch foaming equipment: the mini-batch, J. Cell. Plast. 52 (2016) 533–543, https://doi.org/10.1177/0021955X15584654.

[24] M.R. Di Caprio, D. Tammaro, E. Di Maio, S. Cavalca, V. Parenti, A. Fangareggi, S. Iannace, A pressure vessel for studying gas foaming of thermosetting polymers: sorption, synthesis and processing, Polym. Test. 62 (2017) 137–142, https://doi.org/10.1016/j.polymertesting.2017.06.019.

[25] C.B. Park, D.F. Baldwin, N.P. Suh, Axiomatic design of a microcellular filament extrusion system, Res. Eng. Des. 83 (8) (1996) 166–177, https://doi.org/10.1007/BF01608351, 1996.

[26] Y.H. Liu, Z.H. Hu, Z.G. Suo, L.Z. Hu, L.Y. Feng, X.Q. Gong, Y. Liu, J.C. Zhang, High-throughput experiments facilitate materials innovation: a review, Sci. China Technol. Sci. 62 (2019) 521–545, https://doi.org/10.1007/s11431-018-9369-9.

[27] M.A.R. Meier, R. Hoogenboom, U.S. Schubert, Combinatorial methods, automated synthesis and high-throughput screening in polymer research: the evolution continues, Macromol. Rapid Commun. 25 (2004) 21–33, https://doi.org/10.1002/marc.200300147.

[28] Q. Guo, J. Wang, C.B. Park, M. Ohshima, A microcellular foaming simulation system with a high pressure-drop rate, Ind. Eng. Chem. Res. 45 (2006) 6153–6161, https://doi.org/10.1021/ie060105w.

[29] C. Marrazzo, E. Di Maio, S. Iannace, L. Nicolais, Process-structure relationships in PCL foaming, J. Cell. Plast. 44 (2008) 37, https://doi.org/10.1177/0021955X07079147, 44 (2008) Journal of Cellular Plastics.